Investigation on ettringite as a low-cost high-density thermochemical heat storage material: Thermodynamics and kinetics

B. Chen, K. Johannes, L. Ratel, M. Horgnies, V. Morin, F. Kuznik

Investigation on ettringite as a low-cost high-density thermochemical heat storage material: thermodynamics and kinetics

B. Chen[1, 2], K. Johannes[1], L. Ratel[1], M. Horgnies[2], V. Morin[2], F. Kuznik[1, *]

[1] *Univ Lyon, CNRS, INSA-Lyon, Université Claude Bernard Lyon 1, CETHIL UMR 5008, F-69621, Villeurbanne, France*

[2] *LafargeHolcim Innovation Center, 95 rue du Montmurier BP15, 38291 Saint Quentin Fallavier, France*

* Corresponding author. E-mail address: frederic.kuznik@insa-lyon.fr

Abstract

Ettringite-based thermochemical energy storage has been recommended to be used in buildings for thermal energy supply because of its low material cost (< 1000 €/m^3), low working temperature and high energy storage capacity. However, several physicochemical properties of ettringite were still not clear, such as reversible reaction enthalpies, thermodynamic equilibrium, and kinetics of the dehydration/hydration reactions. In this study, the dehydration of ettringite was experimentally confirmed as stepwise in TGA-DSC, Ett30.6 → Ett30 → Met17.8→ Met11.7 → Met7.5, which is consistent with the inference according to the crystal structure. The thermodynamic equilibrium of the reversible reactions presented the impact of water activity on the stability of ettringite at controlled temperatures and water vapor partial pressures. The thermodynamic modeling based on experiment results is consistent with the extrapolated model from the literature. The rehydration enthalpy of ettringite has been confirmed about 1370 kJ/mol, which equals an energy density of 547 kWh/m^3 under the operating conditions of 20 °C and 90 % RH.

Key words: de/re-hydration, ettringite, thermodynamic equilibrium, thermochemical energy storage, reaction kinetics

Abbreviation

dHF	Derivation of heat flow [mJ/s^2]
DSC	Differential scanning calorimetry
EttX	Ettringite contained X H_2O molecules
MetX	Meta-ettringite contained X H_2O molecules
PWVP	Partial water vapor pressure [Pa]/[mbar]
RH	Relative humidity (%)
SSA	Specific surface area
TGA	Thermogravimetric analysis
XRD	X-ray diffraction analysis

Latin symbols

Cp	Specific heat capacity [J/(kg·K)]
K_{eq}	Equilibrium constant
m	Mass of sample [mg]
Δm	Mass change [mg]
M	Molar mass [g/mol]
n	Calculated water molecule number
P	Pressure (Pa)
P^0	Standard atmosphere pressure (100 kPa)
R	Ideal gas constant, 8.3145 J/(mol·K)
R^2	Coefficient of determination
T	Temperature [K]
X	Water molecule number
ΔG	Change in Gibbs free energy [kJ/mol]

ΔH	Change in reaction enthalpy [kJ/mol]
ΔS	Change in reaction entropy [J/(K·mol)]

Subscripts

eq	Equilibrium
H_2O	Water
i	Initial
r	Reaction
sorp	Sorption
0	Standard conditions

1 Introduction

Improving the efficiency of thermal energy use is always a hot topic in the industry and the building sector. Comparing to cut down direct consummation of heating, new options of providing extra energy from solar energy seem to be more acceptable to residents without influencing comfort. However, there exists a geographic and time mismatch between the supply and demand of solar energy. Thermal energy storage technologies aim indeed at getting rid of this shift. Thermal energy storage materials could be divided into sensible heat, latent heat, and sorption storage materials. Among them, chemical sorption materials are very promising thanks to their high energy storage densities and little heat losses during storage, especially if the storage duration is long [1,2].

Previous researches on thermochemical storage materials have mainly focused on inorganic salts hydrates [2]. Whereas, only several of salts, such as $MgSO_4$, $SrBr_2$, and $LaCl_3$, are classified as promising mediums for thermal energy storage [3]. Salts being commonly in form of powder, the agglomeration of particles and over-hydration are very impedimental during hydration. Moreover, high material cost only allows laboratory-scale tests rather than real, large scale, application use. Recently, composite materials based on ettringite, who could overcome the above hindrances easily, were proposed in several investigations [4–9]. As a material in the hydrated cement paste, the form of samples can be easily controlled and its material cost (< 1000 €/m^3) is lower than other common thermal energy storage materials, like Silica gel (4300 €/m^3), Zeolithe 13X (3000 €/m^3), and $SrBr_2$ hydrate (42 000 €/m^3) [9]. The comparable energy density (500 kWh·m^{-3} [7]) of ettringite with salts [2,3] promises a small volume for heat storage. Additionally, reported low work temperature of 60 °C [7,10] makes ettringite suitable for storing low-temperature heat resources like household evacuated tubes panels, industrial waste heat, wind power, off-pick electricity, district heating networks, etc.

1.1 Dehydration of ettringite

Up to now, dehydration kinetic investigations of ettringite ($3CaO·Al_2O_3·3CaSO_4·32H_2O$) have been carried out in the nitrogen atmosphere. The partially dehydrated ettringite is termed as meta-ettringite ($3CaO·Al_2O_3·3CaSO_4·nH_2O$, $n \neq 0$) which contains various water molecules numbers (n in the **Eq.1**) ranging between 8 and 13 [9], which correspond 27.2–34.4 % of weight loss for the 32-hydrate ettringite. However, reported dehydration temperatures and enthalpies varied from one study to another (Tab. 1). Grounds et al. [11] identified 21–22 water molecules lost up to 70 °C and another 9–10 H_2O between 70 and 1000 °C for

synthesized 30.7-hydrate ettringite in Thermogravimetric analysis (TGA). Struble and Brown [12] measured the dehydration enthalpy for the dehydration at 30–70 °C at 753 kJ/mol along with a thermal capacity (Cp) of 1.3 $J \cdot g^{-1} \cdot K^{-1}$ by Differential Scanning Calorimetry (DSC). Alternatively, the investigation by Ings and Brown [13] presented the endothermic process of 1097 kJ/mol located at 67–122 °C, while reported in [7], the dehydration enthalpy was 1024 kJ/mol at 60 °C and 1233 kJ/mol at 65 °C. The dehydration process was supposed to be stepwise according to the crystal structure of ettringite [14–16]. However, this stepwise dehydration process has not been proved in numerous thermal characterization analyses (TGA and DSC) on ettringite [7]. On the other hand, the loss of 12 H_2O at 40 °C in N_2 flow was said to not impact the specific surface area (SSA) of ettringite. While at higher temperatures than 50 °C, loss of more than 14 H_2O made the SSA increased with crystallinity down [17]. Detailed work by Baquerizo et al. [7] demonstrated that the dehydration conditions of 30-hydrate ettringite was given by $RH = 0.327 + 0.108T - 0.002T^2 + 4.8\times10^{-5}T^3$. Moreover, ettringite could experimentally lose its crystallinity at 60 °C and 0 % relative humidity (RH). Similar phenomena were also observed on ettringite-based cement paste materials at high temperatures (inferior to 100 °C) and low relative humidity (RH, 0–8 %) [4,5,18].

$$3CaO \cdot Al_2O_3 \cdot 3CaSO_4 \cdot 32H_2O \xrightarrow{\Delta} 3CaO \cdot Al_2O_3 \cdot 3CaSO_4 \cdot nH_2O + (32-n)H_2O\ (g)$$

(**Eq. 1**)

1.2 Hydration of meta-ettringite

Hydration of meta-ettringite, the reverse process of dehydration of ettringite, could make the short-range order of meta-ettringite crystals (amorphous) reform long-range order of ettringite (crystal) at above 60% RH [18,19]. After several dehydration/hydration cycles, ettringite was still able to be reformed from meta-ettringite that dehydrated at 40 °C and 0 % RH [12]. The water content of reformed ettringite depended on the dehydration degree [14] and hydration relative humidity (or partial water vapor pressure, PWVP) [7,12,20]. The hydration enthalpies of meta-ettringite and the evolution of water molecule number by liquid water and water vapor are summarized in Tab. 1 for different investigations [9]. Not only pure meta-ettringite [7,12,20] but also meta-ettringite in composite materials [4,5,9,18] have been proved to be reversible. However, the reversible reaction was accompanied by a very significant hysteresis [7,20]. In other words, the reformation of ettringite went under a relatively higher water vapor pressure compared with that of the decomposition process at the same temperature, or lower temperature at the same PWVP. Numerically, the boundary

conditions for hydration of the 13-hydrate meta-ettringite was modelled as RH = 56.608 + 0.186T + 0.001T^2 [7]. During the hydration, the process was believed as stepwise [7]: Step 1: From n = 9 to 13, the average enthalpy is equal to – 60.5 kJ/mol H_2O; Step 2: From n = 13 to 30, ΔH_{sorp} = – 57.3 kJ/mol H_2O; Step 3 is the sorption of last 2 zeolitic water molecules between the crystal columns (ΔH_{sorp} = – 50.0 kJ/mol H_2O). Hereby, the total exothermic sorption process for hydration gave 1316.1 kJ/mol ettringite (Tab. 1). However, this enthalpy of hydration decreased to 286 kJ/mol (ΔH = – 12.4 kJ/mol H_2O, Tab. 1) when hydrated by liquid water [7]. The difference was due to the condensation enthalpy of water vapor.

Table 1. Different dehydration and hydration reactions for ettringite and corresponding enthalpies extracted from [9].

Process	Reaction	ΔH (kJ/mol)	ΔH (kJ/mol H_2O)	Weight of Samples (powder)	Reference
Dehydration	Ett32 (s)→ Met12 (s)+ 20H_2O(g)	+ 630	+ 31.5	~ 1 mg	[21]
		+ 1135	+ 56.7	/	[7]
	Ett32 (s)→ Met13 (s)+ 19H_2O(g)	+ 753 (±126)	+ 39.8 (±6.6)	~ 1 mg	[12]
		+ 1074	+ 56.5	/	[7]
	Ett31 (s)→ Met9.3 (s)+ 21.7H_2O(g)	+ 1204 (60 °C)	+ 55.5	5.53 mg	[7]
	Ett31(s)→ Met8.7 (s)+ 22.3H_2O(g)	+ 1233 (65 °C)	+ 55.2	8.93 mg	[7]
Hydration	Met15.5 (s)+ 16.5H_2O (l)→ Ett32(s)	– 241	–14.6	Several grams	[21]
		– 205	– 12.4	/	[7]
	Met10.5 (s)+ 21.5H_2O (l)→ Ett32(s)	– 385	– 17.9	Several grams	[21]
		– 279	– 13.0	/	[7]
	Met11 (s)+ 21H_2O (l)→ Ett32(s)	–238.5	– 11.4	38–50 mg	[7]
	Met9 (s)+ 23H_2O (l) → Ett32(s)	– 286	– 12.4	492 mg	[7]
	Met 9(s)+ 23H_2O (g) → Ett32(s)	– 1316.1	– 57.2	~ 80 mg	[7]

Current researches have proved the possibility of using low-cost ettringite materials for thermal energy storage. However, most key properties of ettringite are still unclear. The alleged stepwise dehydration and hydration in terms of theoretic ettringite structure are not experimentally proved. In the meantime, the dehydration enthalpies are not identical in the literature. Besides, the hydration demands an extra humidity resource, which could be economically beneficial if the heat release takes place under near-boundary conditions (e.g. thermodynamic equilibrium). Nevertheless, no detailed dynamic and kinetic studies are

accessible for de/re-hydration of ettringite that showing the possible evolution of water molecule number in per phase of ettringite. Therefore, in the present investigation, the dehydration and rehydration of pure ettringite are supposed to be systematically explained to conclude the thermodynamic equilibrium. Moreover, the kinetics of de- and hydration of ettringite and corresponding enthalpies are studied at charging and discharging conditions according to thermodynamic equations.

2 Materials and methodology

2.1 Preparation of materials

Aiming at obtaining ettringite of high purity, all reagents used were analytical grade. Calcite was firstly calcined at 1000 °C for 4 h. Once no carbonate in the solid confirmed by XRD, the prepared CaO was then dissolved in fresh cold CO_2-free distilled water. The saturated $Ca(OH)_2$ solution was then mixed with $Al_2(SO_4)_3 \cdot 14H_2O$ (8.2 wt.% Al_2O_3) under the string and N_2 protection at 10 °C for 2h to produce ettringite crystals. After decanting for 3 days, the precipitates were vacuum filtered and washed by cold distilled CO_2 free water and ethanol for two times. At last, the purity of ground solids was defined by XRD and the remains were stored in a desiccator containing saturated $CaCl_2$ solution and N_2 for later use.

2.2 Characterization methods

2.2.1 Particule size

From laser granulometry analysis, the ground synthetic ettringite powder is mostly smaller than 125 µm. The mean diameter is about 28 µm.

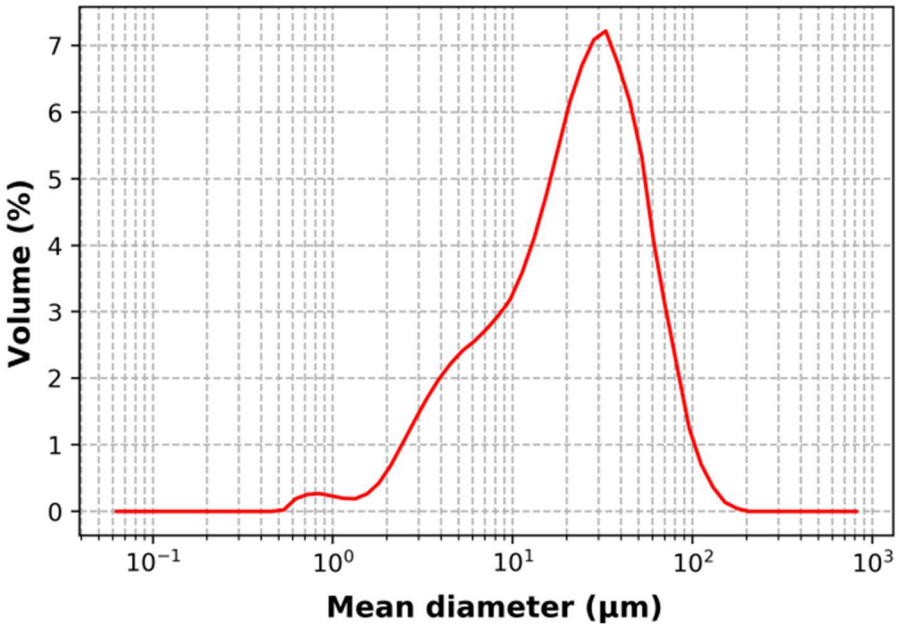

Figure 1. Size distribution of ettringite particles.

2.2.2 TGA

The thermal stability of ettringite was characterized by TGA (Mettler TGA/DSC 3+) from 30 to 1000 °C with a heating rate of 10 K/min under a nitrogen flow of 20 ml/min. The quantity of water and carbonate in the samples were then determined thanks to different decomposition temperatures. The water molecule number in per mole of ettringite could be calculated by **Eq. 2** with the assumption of a perfect metal oxides structure ($3CaO{\cdot}Al_2O_3{\cdot}3CaSO_4$) before 550 °C:

$$n = \frac{(m_i - m_{550\,°C})}{M_{H2O}} \Big/ \left(\frac{m_{550\,°C}}{M_{metal\ oxides}}\right) \quad \textbf{(Eq. 2)}$$

Where m_i is the initial mass of sample in TGA, M is the molar mass of substances and n is the water molecule number.

The dehydration and hydration processes were monitored by TGA-DSC (Sensys Evo TG-DSC, Setaram Instrument) coupling with a gas humidity generator (Wetsys, Setaram Instrument). The micro-balance of the instrument was protected by helium. For dehydration, certain amounts of samples were heated at different temperatures with 10 K/min under target humidities controlled by Wetsys with an N_2 flux of 50 ml/min. In terms of hydration, meta-ettringite was firstly produced by dehydrating ~3 mg of ettringite at 80 °C then cooled down to set hydration temperature in dry N_2 environment. Once the temperature stabilized, the humidity generator injected humid N_2 flow containing the target quantity of water vapor into the TGA-DSC for hydrating meta-ettringite. During the thermodynamic experimentations, the end of each process is defined as: the variation of weight is less than 0.04 % during the last hour. It should be noticed that the Wetsys needed about 20 minutes to reach the set values. During all processes, the evolutions of sample masses were continuously recorded. The same white experiments were executed for every thermal characterization. Thanks to the variation of mass, water molecule number in per ettringite molecule could be extrapolated, neglecting the trace of impurities, by:

$$n_{H2O} = \frac{\Delta m / M_{H2O}}{m_i / M_{ettringite}} \quad \textbf{(Eq. 3)}$$

Where Δm is the variation of mass during certain operations in TGA. The hydration advancement could be inferred as:

$$\textbf{Hydration advancement} = \frac{m_{water\ gain}}{m_{ettringite} - m_{meta-ettringite}} \quad \textbf{(Eq. 4)}$$

2.2.3 XRD

X-ray diffraction analysis (XRD) used in this contribution was to follow the phase assemblage. It was equipped with a Philips/PANalytical X'Pert Pro-MPD Powder Diffractometer with an X'Celerator detector (CuKα radiation beam, 40 kV and 40 mA). The scanned range is between 2θ = 5–65 ° by a step of 0.25 ° for 40 min in the ambient environment.

2.3 Calculation for thermodynamic equilibrium

The variation of Gibbs free energy for a chemical reversible process could be expressed as $\Delta_r \boldsymbol{G^0} = -\boldsymbol{RT}\ln \boldsymbol{K_{eq}}$. The equilibrium constant $\boldsymbol{K_{eq}}$ of **Eq. 1** could be simplified as $\boldsymbol{K_{eq}} = \left(\boldsymbol{P_{eq}}(\boldsymbol{H_2O})/\boldsymbol{P^0}\right)^{\boldsymbol{32-n}}$. For a reaction at constant temperature and pressure, the Gibbs free energy equation can also be specified in terms of changes in enthalpy and entropy $\Delta_r \boldsymbol{G^0} = \Delta_r \boldsymbol{H^0} - \boldsymbol{T}\Delta_r \boldsymbol{S^0}$. Hereby the correlation of water vapor and temperature for the thermodynamic equilibrium of dehydration and hydration processes is extracted as **Eq. 5** at $\boldsymbol{P^0} = \boldsymbol{100\ kPa}$:

$$\ln \boldsymbol{K_{eq}} = \ln\left[\left(\frac{\boldsymbol{p_{eq}}(\boldsymbol{H_2O})}{\boldsymbol{p^0}}\right)^{\boldsymbol{32-n}}\right] = -\frac{\Delta_r \boldsymbol{H^0}}{\boldsymbol{RT_{eq}}} + \frac{\Delta_r \boldsymbol{S^0}}{\boldsymbol{R}} \quad \textbf{(Eq.5)}$$

Thus,

$$\ln \boldsymbol{P_{eq}}(\boldsymbol{H_2O}) = -\frac{\Delta_r \boldsymbol{H^0}}{\boldsymbol{(32-n)RT_{eq}}} + \frac{\Delta_r \boldsymbol{S^0}}{\boldsymbol{(32-n)R}} + \ln \boldsymbol{P^0} \quad \textbf{(Eq. 6)}$$

The van't Hoff plot of **Eq. 6** demonstrates that the logarithmic water vapor pressure is linearly proportional to $\frac{\boldsymbol{1}}{\boldsymbol{T_{eq}}}$ with the slop of $-\frac{\Delta_r \boldsymbol{H^0}}{\boldsymbol{(32-n)R}}$ and intercept of $\frac{\Delta_r \boldsymbol{S^0}}{\boldsymbol{(32-n)R}} + \ln \boldsymbol{P^0}$.

3 Results and discussion

3.1 Material characterization

The purity of synthesized ettringite is 99.6 % with a trace of $Al(OH)_3$ and $Ca(OH)_2$. No calcium carbonate is detected in XRD (Fig. 2 a), which is also confirmed in the TGA result: no peak locates between 550 and 1000 °C (Fig. 2 b) where carbonates are supposed to decompose. The synthetic sample undergoes a total weight loss of 44.8 % (till 1000 °C). Therefore, the synthesized ettringite phase averagely contained 30.6 water molecules

(chemical formula: $3CaO{\cdot}Al_2O_3{\cdot}3CaSO_4{\cdot}30.6H_2O$), neglecting the impurity traces. The dehydration could be mainly divided into two stages of water removal. The first step occurs between 30–200 °C with a loss of 36.3 %, which corresponds to 24.8 water molecules. The maximum water removal rate locates at around 130 °C. At the second stage, between 200 and 550 °C, the water loss is 7.9 %, equivalent to 5.4 H_2O.

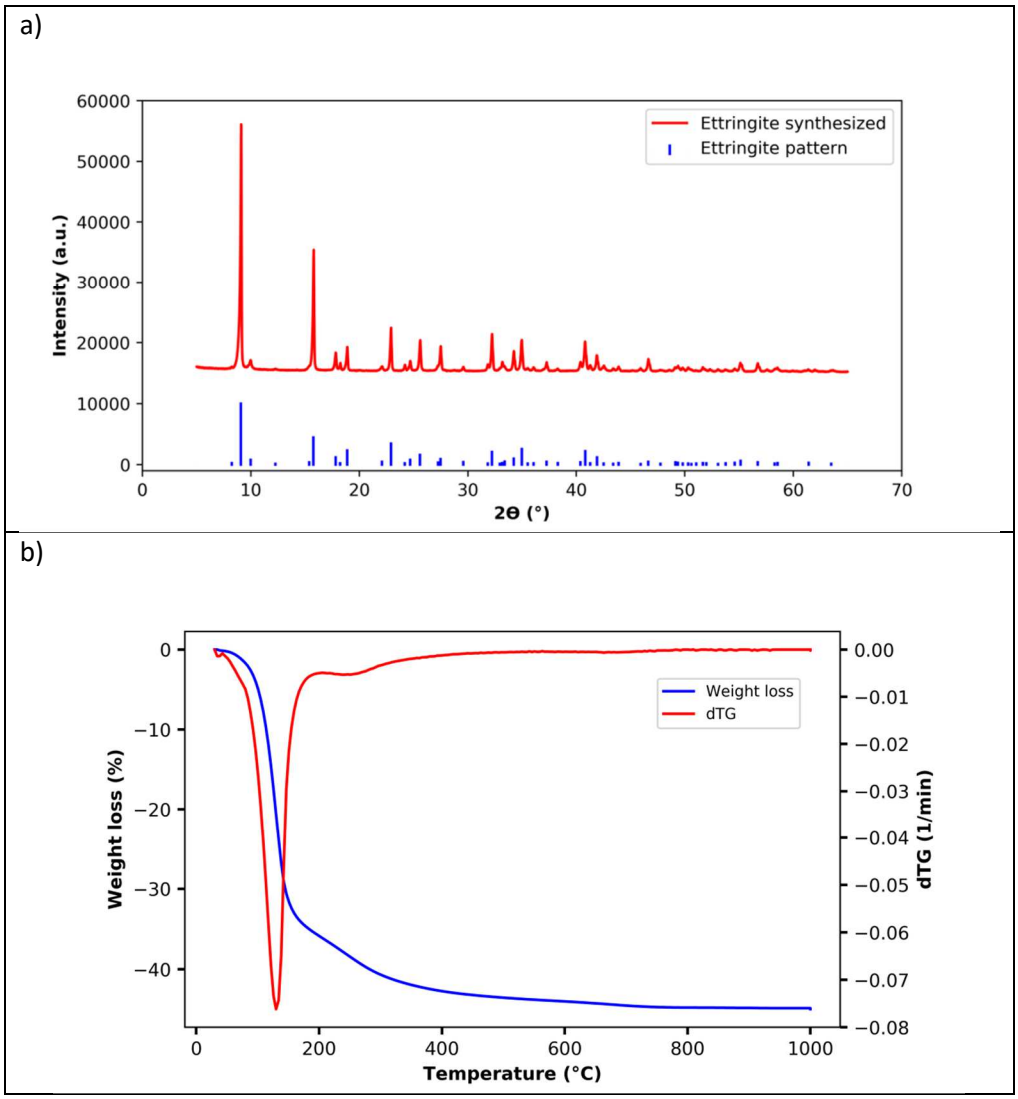

Figure 2. XRD (a) and TGA (b) analysis of synthetic ettringite.

3.2 Kinetics of dehydration and rehydration of ettringite

3.2.1 Temperature and mass effect on dehydration

Fig. 3 a represents the weight loss curves during isothermal dehydration in dry nitrogen for around 10 mg ettringite at different temperatures. The dehydration mostly occurs during the first hour. A higher dehydration temperature leads to a faster dehydration process and higher mass loss. The results are very reproducible at the same dehydration temperature (80 °C). Additionally, a small quantity of samples could accelerate the dehydration behavior

but with a similar final water loss level (Fig. 3 b). The analysis results about dehydration are detailed in Tab. 2. The enthalpies, that are proportional to the loss of water molecule number, stabilize around 1260 kJ/mol. It should be noted that the dehydration continued slowly after 15 hours in a dry nitrogen environment. However, the rate is very low and the heat flow is too small to be detected (see in Fig. 4). Considering the rate of dehydration and also the possible damage of the column structure of ettringite caused by high temperature, the dehydration temperature and sample mass are settled at 80 °C and 3 mg for the remaining experiments presented in this article. Moreover, under humid N_2, the increase of PWVP only decreases slightly dehydration rate and degree at 80 °C (Fig. 3 c); because the variation of RH from 4 to 12 mbar H_2O (g) is very little, from 0.8 to 2.6 % RH. Comparing to the 34.1% weight loss at 80 °C in dry N_2, the dehydration at 8 mbar H_2O (g) leads to a lower level of 31.2 %.

Table 2. Summarization of isothermal dehydration of ettringite in dry N_2 flux.

Dehydration temperature (°C)	Mass of sample (mg)	Mass loss (%)	Number of residual water molecules	Enthalpies (kJ/mol)
60	10.32	32.2	8.6	1248
80	10.76	33.8	7.5	1241
	10.30	33.5	7.7	1262
	6.70	33.9	7.4	1257
	3.18	34.1	7.3	1290
100	10.48	36.2	5.9	1348

a)

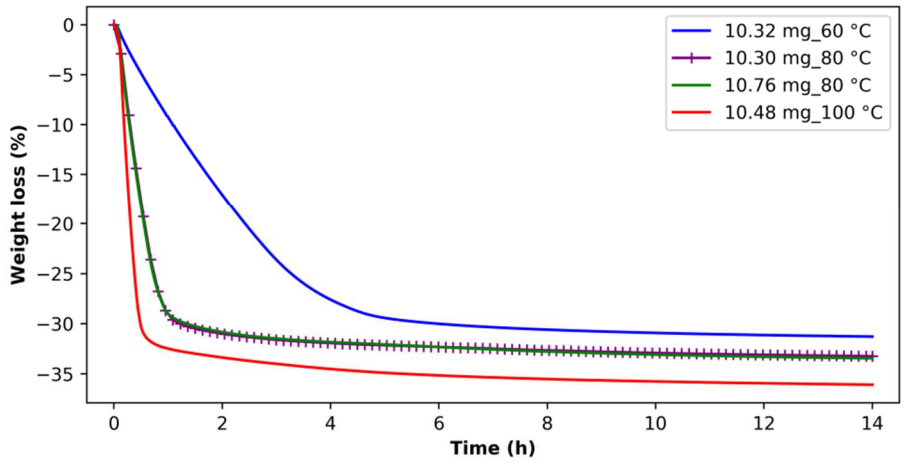

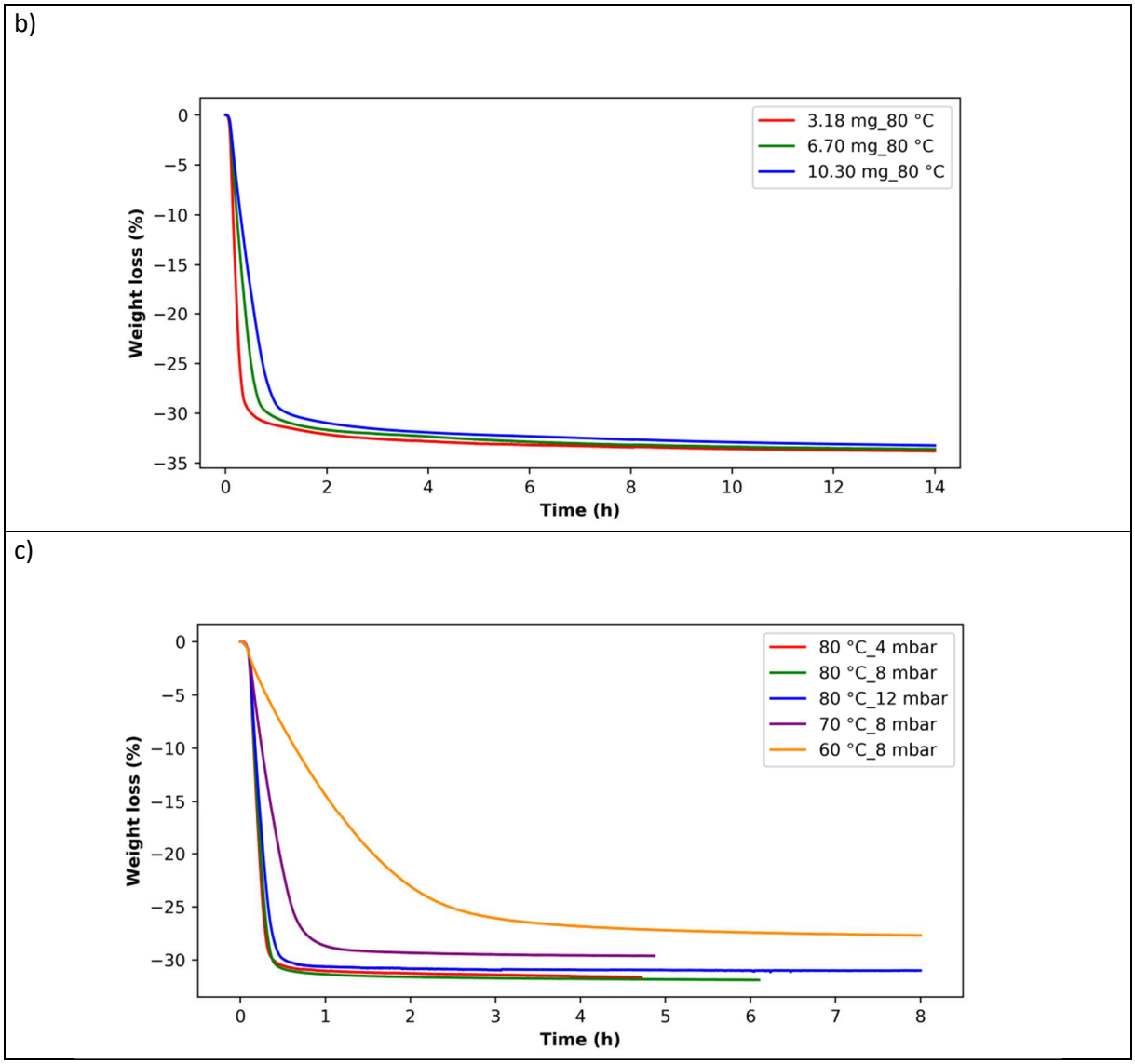

Figure 3. Dehydration behavior of ettringite under effects from: dehydration temperature (a, dry N_2), mass (b, dry N_2) and PWVP (c, humid N_2).

3.2.2 Stepwise dehydration process

Given by Fig. 4, the profile of isothermal weight loss curve demonstrates that, the main loss of weight is very continuous without any plateau. However, the peaks on the curve of heat flow derivation (dHF) indicate the rate variation of heat-consuming during the endothermic process at 80 °C in TGA-DSC. The endothermic heat flow change is supposed to be caused by the rupture of different chemical bonds of hydroxyl groups on calcium and oxygen atoms. According to the positions of dHF peaks on time, the weight loss could be separated into four parts corresponding to different losses of water molecule numbers (Tab. 3). This process is consistent with theoretical inference in [14–16]. To remove the residual water molecules, a higher dehydration temperature is required. It should be noted that this stepwise

dehydration is not like a mono-variant system: no clear boundaries (plateaus) have been detected for each step in the TGA signal.

Table 3 Experimental confirmation on the stepwise dehydration process of ettringite at 80 °C in N_2 flow.

Theoretical inference [14–16]			**Experimental results in this study**	
Component description	Number of removed water molecules	Location	Component description	Number of removed water molecules
$3CaO{\cdot}Al_2O_3{\cdot}3CaSO_4{\cdot}\mathbf{32}H_2O$			$3CaO{\cdot}Al_2O_3{\cdot}3CaSO_4{\cdot}\mathbf{30}.6H_2O$	
$3CaO{\cdot}Al_2O_3{\cdot}3CaSO_4{\cdot}\mathbf{30}H_2O$	2	Inter-column channel	$3CaO{\cdot}Al_2O_3{\cdot}3CaSO_4{\cdot}\mathbf{30}H_2O$	0.6
$3CaO{\cdot}Al_2O_3{\cdot}3CaSO_4{\cdot}18H_2O$	12	In the additional vertices of the trigonal prisms	$3CaO{\cdot}Al_2O_3{\cdot}3CaSO_4{\cdot}17.8H_2O$	12.2
$3CaO{\cdot}Al_2O_3{\cdot}3CaSO_4{\cdot}12H_2O$	6	In the main vertices of the trigonal prisms.	$3CaO{\cdot}Al_2O_3{\cdot}3CaSO_4{\cdot}11.7H_2O$	6.1
$3CaO{\cdot}Al_2O_3{\cdot}3CaSO_4{\cdot}6H_2O$	6		$3CaO{\cdot}Al_2O_3{\cdot}3CaSO_4{\cdot}7.5H_2O$ (dehydration process not completed)	4.2
$3CaO{\cdot}Al_2O_3{\cdot}3CaSO_4$	6	Al and Ca polyhedral	N/A	N/A

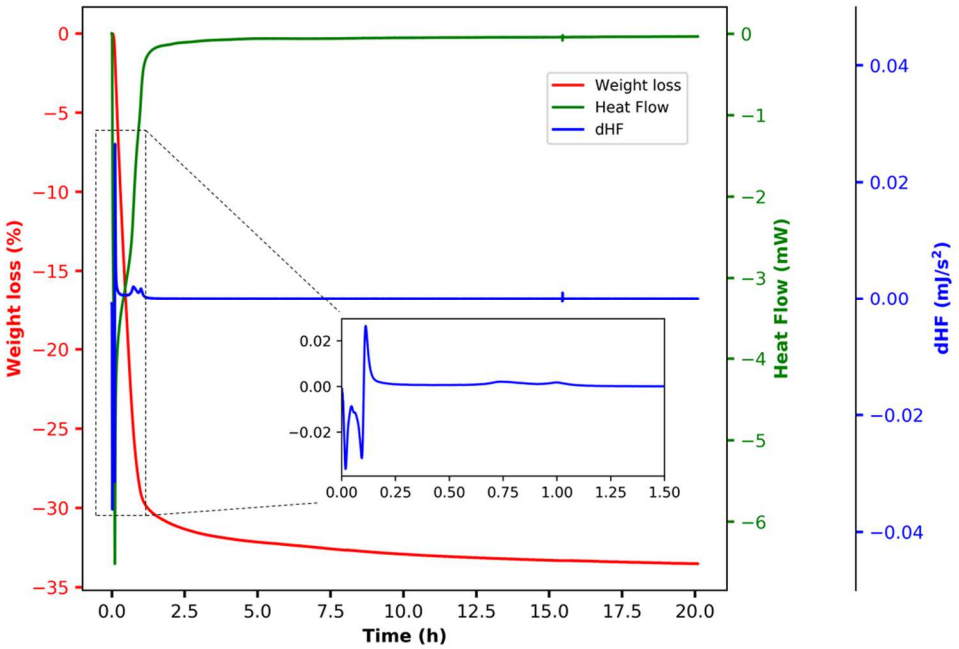

Figure 4. Possible stepwise dehydration process at 80 °C (dry N_2).

3.2.3 Rehydration enthalpy of meta-ettringite

Fig. 5 presents the hydration profile of meta-ettringite (from 2.96 mg ettringite as calculation reference) at 20°C and 21 mbar PWVP in order to complete the reversible reaction. During the first 30 minutes, the sorption of water vapor was very rapid given by the slope of curve "degree of hydration advancement" and the instantaneous heat release power could reach up to 1.4 mW. Then the heat flow decreased to about 0.3 mW with a linear increase of mass. After about 2.5 hours, the hydration slowed down and heat release trended to 0 progressively. At 7 hours, the heat liberated by the sorption of water vapor was too weak to be detected by the instrument. The final level of the hydration advancement for ettringite stabilized at 1.14 which could be converted to around 40 % for weight gain. About 6 % extra weight growth is due to over-hydration compared to mass loss during dehydration. The over-hydration owns to adsorption of zeolitic water molecules which could be as many as 6 instead of 2 in normal ettringite crystal [22]. The cumulated enthalpy of the hydration process is 1370 kJ/mol for forming Ett32.4. This real value is indeed bigger since the continuous absorption of 3.6 water molecules, during which the water molecule number in ettringite increases from 32.4 to 36 (n = 32.4 → 36). However, due to the limitation and incertitude of measurement, the extra heat released is not counted. This kind of over absorption is found in all rehydration experiments if the RH > 76% (Fig. 6). Moreover, the degree of over absorption depends on water vapor pressure. The higher the water vapor is, the more significant the over-hydration. The rate of hydration is similar when hydration advancement inferior to 0.12, which may be attributed to the absorption of water vapor at the surface of particles. Then, it depends on the chosen conditions, like temperature and water vapor pressure. The results about rehydration experiments are concluded in Tab. 4.

Table 4. Hydration enthalpies and regained water molecule number at different conditions.

Hydration temperature (°C)	Water vapor pressure (mbar)	Initial Weight of sample (mg)	Water molecule loss	water molecules gained	Final water molecule number	Enthalpies* (kJ/mol)	Enthalpies (kJ/mol H_2O)
25	27	2.48	22.8	28.1	35.9	1330 (29.6)	60.9
22	20	2.44	23.7	24.4	31.1	1058 (25.8)	55.9
20	21	2.96	23.9	27.4	34.1	1370 (32.4)	53.3
	20	2.84	23.9	27.0	33.7	1341 (31.8)	53.5
	19	2.82	23.8	27.2	33.9	1214 (28.5)	55.9

* The value the in bracket presents the water molecule number in the reformed phase for the corresponding enthalpy.

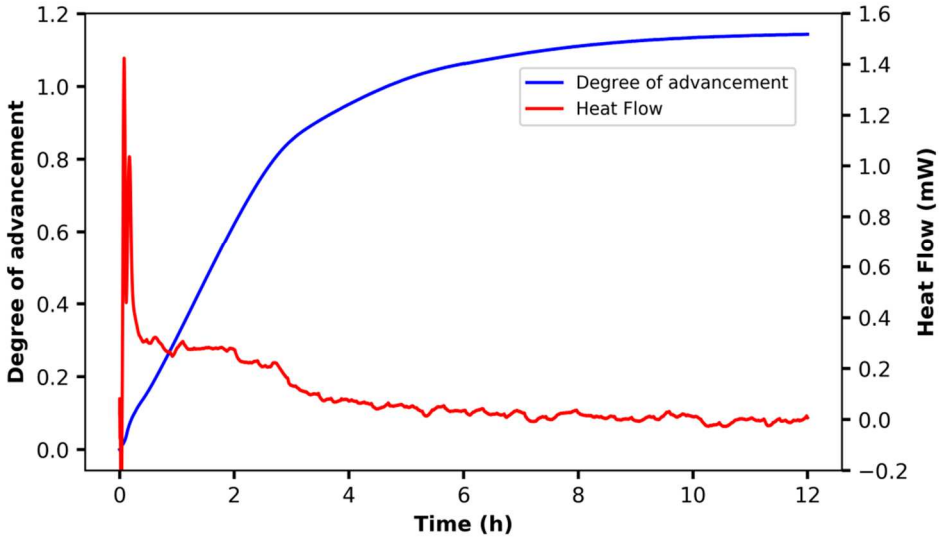

Figure 5. Hydration of meta-ettringite at 20°C and 21 mbar (90 % RH).

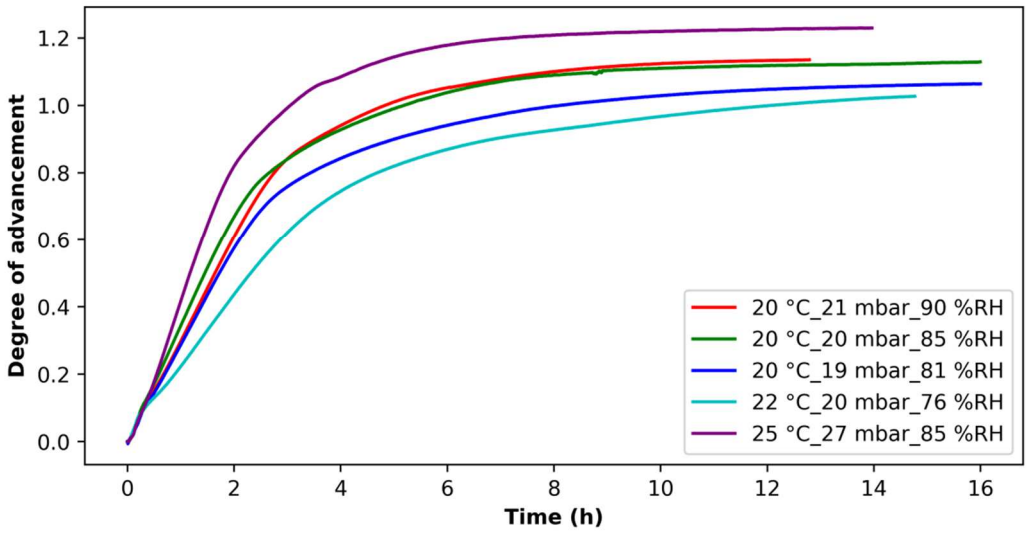

Figure 6. Hydration of meta-ettringite at various temperatures and PWVPs.

3.3 Thermodynamic equilibrium

3.3.1 Dehydration of ettringite

The dehydration of ettringite refers to the loss of zeolitic water in the channel structure and chemically bonded water in the column structure. The number of water molecules (n) in per ettringite and meta-ettringite phases were obtained from several experiments under the ranges of 25–80 °C and 0 (dry N_2 environment)–32 mbar. Fig. 7 shows the

corresponding results of water molecule numbers as a function of temperature and PWVPs. The PWVPs, at which ettringite (Ett30) starts to dehydrate, are different at various temperatures. The higher the temperature is, the bigger the water vapor pressure. At ambient temperature (25 °C), ettringite is stable at P_{H2O} as low as 1 mbar (3.2 % RH). Then it dehydrates very slowly to a 13.2-hydrate at 0.3 mbar (1 % RH) for more than one week in TGA-DSC. When temperature increases to 50 °C, ettringite is at P_{H2O} down to 8 mbar, similarly 14 mbar for 55 °C and 20 mbar for 60 °C. Before these PWVPs, the loss of weight is due to the removal of zeolitic water in the channels between ettringite column structures. After these PWVPs, it has been observed that weight loss varies for each change of the PWVPs. The sample shows a bi-variant behavior during the dehydration at 50, 55, and 60 °C at low PWVPs. The equilibrium values of weight loss depend on both temperature and PWVP. Systematic repetitions of experiments have been performed in order to verify whether the obtained experimental values of weight loss corresponded to equilibrium values. At 70 °C and 80 °C, ettringite dehydrates directly to meta-ettringite under given conditions. The water molecule number in the dehydrated phases are respectively 12.6 for 70 °C at 28 mbar and 8.8 for 80 °C at 32 mbar. This could be explained by that the dehydration energy given is higher than the activation energy of thermodynamic equilibrium to form intermediates observed at 50–60 °C.

Seen from the results of water being regularly removed at 50, 55, and 60°C, the slope break of curves, locating at $n \approx 12$, indicates a different mechanism of losing water molecules before and after this point. When n is higher than 12, the absolute value of the slope of curves is bigger than the one of $n < 12$, which means a relatively smaller activation energy needed to remove water molecules until equal to 12. According to [14–16], after the removal of 18 water molecules from Ett30 to Met12, there still remains 6 H_2O bound in the Ca polyhedral of the columns. Comparing to the former bond length of Ca-OH in Ett30, this interatomic distance could be shorter due to the arrangement of structure for a smaller coordination number of Ca. This reorganization may increase the dehydration activation energy for water molecules remained, which leads to a smaller water molecule number removed when $n < 12$. The n at 0 mbar (dry N_2 environment) is lower than the ones in the section 3.2.1 for kinetic study, eg. here $n = 6$ instead of about 7.5 for dehydration at 80 °C. Because a much longer time is required to achieve the thermodynamic equilibrium. The last 6 H_2O correspond to those molecules bonded in the

Al and Ca polyhedral [14–16], which means more energy (a higher temperature) is necessary to make them detached than other H_2O in the ettringite crystal.

Overall, four zones can be distinguished in Fig. 7. The first zone is characterized by the continuous removal of zeolitic water of the ettringite. The second zone (light-redden area in Fig. 7) at low temperature (curve at 25 °C) and low water vapor pressure where there is no equilibrium points and can be interpreted as a mono-variant zone (see more in the Section 3.3.2). The isotherm at 25 °C is step-shaped meaning that the water vapor pressure of dehydration transformation in this zone is a function of the temperature. In the third zone, at higher temperatures (50–60 °C) and higher water vapor pressure (3–22 mbar) for $13 < n < 30$, the continuous change of the water molecule number with water vapor pressure. Finally, the fourth zone is characterized by the continuous change of water molecules ($6 < n < 13$) with the water vapor pressure for a fixed temperature. This zone can be interpreted as the stability domain for the meta-ettringite phase.

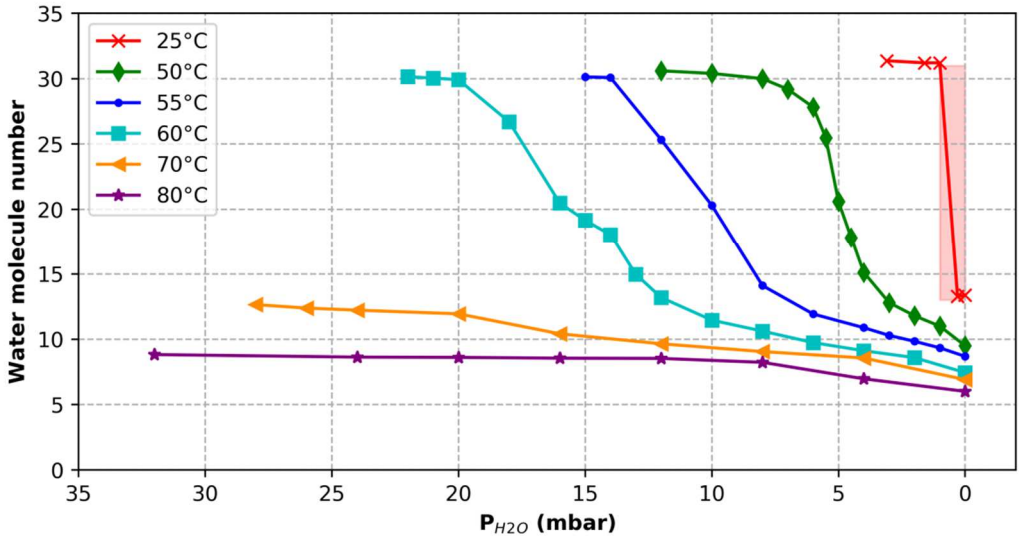

Figure 7. Evolution of water molecule number in ettringite/meta-ettringite during the dehydration at various temperatures and water vapor pressures.

3.3.2 Rehydration of ettringite

After being dehydrated to meta-ettringite, the rehydration of ettringite is executed at different temperatures with the continuous growth of water vapor pressures (Fig. 8). At 15 °C, the start point of meta-ettringite is n = 7.4. Once water pressure is presented, the water molecule number per phase increases gradually to 12.1 until P_{H2O} = 8 mbar. Then a plateau is formed between 8 and 10 mbar for Met12.2. After that, a sharp rise is observed

even the very small step of the water pressure set (0.2 mbar). The next change point seems to locate at 11 mbar (n = ~ 23) and water vapor is then absorbed steadily to produce higher hydrates. Comparing with the rehydration at 15 °C, the n increases regularly but more slowly at 20 °C due to a higher hydration temperature. A similar plateau of n ~ 12 is observed between 12 and 14.5 mbar. After the sudden increase to n = 23 at 15 mbar, the slope of rising reduces at the interval of 15–19 mbar. Differing in the former two cases, the hydration at 25 °C does not reach a plateau after the slow absorption of water vapor to arrive n = 13. After n_{H2O} equivalent to 24, a bigger water vapor pressure step is necessary to make a similar increase in water molecule number in the phase than the ones at 15 and 20 °C. As has been expected, the regular increase of the n has been observed at 30 °C until 25 mbar but the value of n = 12 is not achieved because of required high water vapor pressures.

To summarize, the rehydration process can be separated to different steps according to the slope breakpoints: 1) similar to the results of dehydration of ettringite, the water molecules number changes ($7.4 < n < 12$) are observed for each change of the water vapor pressure in the meta-ettringite domain of stability; 2) dramatic increase step to yield a 24-hydrate without any equilibrium points, indicating that the water vapor pressure of a hydration transformation in this zone is a function of the temperature; 3) the last step to form higher hydrate ettringite for $24 < n < 32$ which can be characterized by a slow kinetic of a reformation of Ett30 [7].

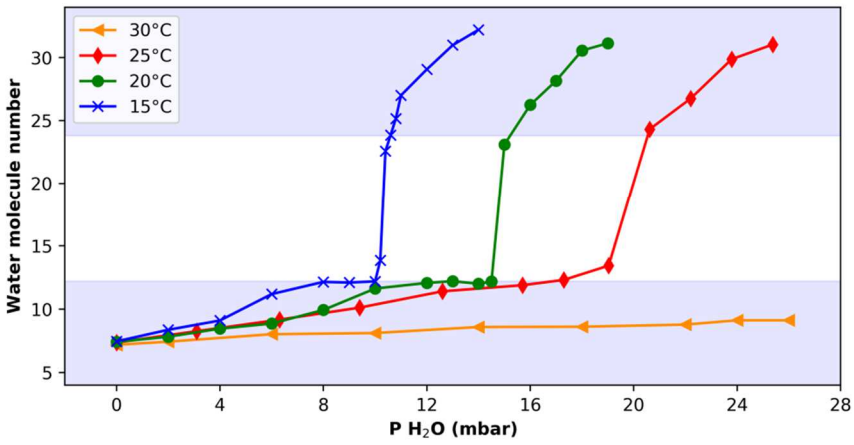

Figure 8. Evolution of water molecules number in the phases during the hydration at various temperatures and water vapor pressures.

3.3.3 Thermodynamic equilibrium

Because of the hysteresis between the hydration and dehydration of ettringite [7], the thermodynamic equilibriums are going to be discussed separately for hydration and dehydration. Fig. 9 a) extracts the main results of the thermodynamic equilibrium for hydration of meta-ettringite at different temperatures and PWVPs. The process has been carried out in the hydration direction shown in Fig. 9 a. The water molecule number in the phase increases from 8.4 to 12.2 during the bi-variant behavior. Once stepped in the light-redden zone, it involves a mono-variant change to 23.8-hydrate until to the upper limit of the cyan curve. After that, the samples continue to hydrate in bi-variant behavior including the absorption of zeolitic water. This variation of hydration mechanism is quite different from [7] as mono-variant from the whole process, but similar to the hydration of soluble anhydrite (AIII-$CaSO_4$) to hemihydrate ($CaSO_4 \cdot 0.5H_2O$) [23].

The slopes and intercepts for corresponding curves of hydration are summarized in Tab. 5. The activation energy generally decreases with the increasing n. When the water molecule number in the phase is smaller than 12, the activation energy is around 69.5 kJ/mol H_2O. Then the enthalpy value decreases to about 51.6 kJ/mol H_2O for the corresponding dramatic increase of the hydration in Fig. 8. The absorption of zeolitic water contributes 47.9 kJ/mol H_2O. The total exothermic hydration produces 1226.9 kJ/mol (equivalent to 52.0 kJ/mol H_2O). This value is somehow underestimated because of the difficulty to achieve an exact same level of water molecule number for the thermodynamic equilibrium.

The hysteresis reported in [7] between ettringite dehydration and rehydration has been also identified by comparing the results in Fig 9 a and b. The dehydration temperatures are much higher for the same water vapor pressures for the reversible process in the hydration or a lower water vapor pressure at the same temperatures. The dehydration activation energy increases erratically to 87.4 kJ/mol H_2O when the n decreases. Same as hydration, the ettringite in dehydration is also proved as a bi-variants system with respect to the thermodynamic study. It should note that the result of dehydration at 25 °C seems to be mono-variant from Ett30 to Met13.3. Therefore, it has not been presented in Fig. 9 b and Tab. 5.

In the literature, the physically deduced model by Baquerizo et al. [7] limited the hydration of meta-ettringite occurring as mono-variant behavior for Met13 + 17 H_2O →

Ett30 (partially shown in Fig. 9 a). According to Eq. 6, the mathematical approach is $lnP_{eq} = -5.927 \times 10^{-3}/T_{eq} + 27.34$. In this study, experimental results demonstrate the variation of van't Hoff equations with the increase of water molecule number. Same as mono-variant for 12.2- to 23.8-hydrate, the approach is $lnP_{eq} = -6.627 \times 10^{-3}/T_{eq} + 29.69$ with the respect to Eq. 6. However, for the higher hydrates of 26.7 and 29.9 H_2O (Tab. 5), the results are very comparable. These similar slopes of curves present similar activation energy of hydration. As for the dehydration of Ett30 to Met13 [7], the model equation is concluded as $lnP_{eq} = -9.853 \times 10^{-3}/T_{eq} + 37.06$ (partially shown Fig. 9 b), while $lnP_{eq} = -9.875 \times 10^{-3}/T_{eq} + 37.27$ in this experimental study for ettringite starting to lose structural water. Same as hydration, the dehydration conditions in this investigation are also found stricter than reported in [7]. The curves of different dehydration gather around the physical model as well as hydration curves. It means that once a dehydration temperature of RH given far from equilibrium, these steps could barely be observed. That's why the stepwise dehydration of ettringite is difficult to be proved in the classic experimental studies of TGA and DSC [7,12,13].

Table 5. Thermodynamic equilibrium results during hydration of meta-ettringite.

Processes	n	Slope (-10^3)	Intercept (SI)	R^2	Activation energy $\Delta_r H^0$ (kJ/mol H_2O)
Hydration	8.4	8.402	34.54	0.990	69.8
	9.1	8.423	35.18	0.998	70.0
	11.4	8.266	35.09	0.999	68.7
	12.2-b[1]	6.696	29.93	1.000	55.7
	12.2-m[2]	6.627	29.69	1.000	55.1
	23.8-b[3]	5.709	26.78	1.000	47.5
	26.7	6.034	27.95	0.999	50.2
	29.9	5.889	27.55	0.991	49.0
	31.0	5.758	27.17	0.996	47.9
Dehydration[4]	30.1	9.875	37.27	0.986	82.1
	25.3	10.174	38.06	0.995	84.6
	20.3	10.28	38.22	/	85.4
	13.2	9.442	35.45	0.999	78.5
	11.9	8.890	33.53	0.992	73.9
	10.9	10.08	36.79	0.968	83.8
	9.8	10.08	36.51	0.968	83.8
	8.7	10.51	36.78	0.979	87.4

[1] Upper limits for the bi-variant zone from 7.4 to 12.2 H_2O

[2] Van't Hoff plot for the mono-variant zone from 12.2 to 23.8 H_2O

[3] Lower limits for the bi-variant zone from 23.8 to 32 H_2O

[4] The dehydration results at 25 °C (mono-variant) is not used to the bi-variant behavior

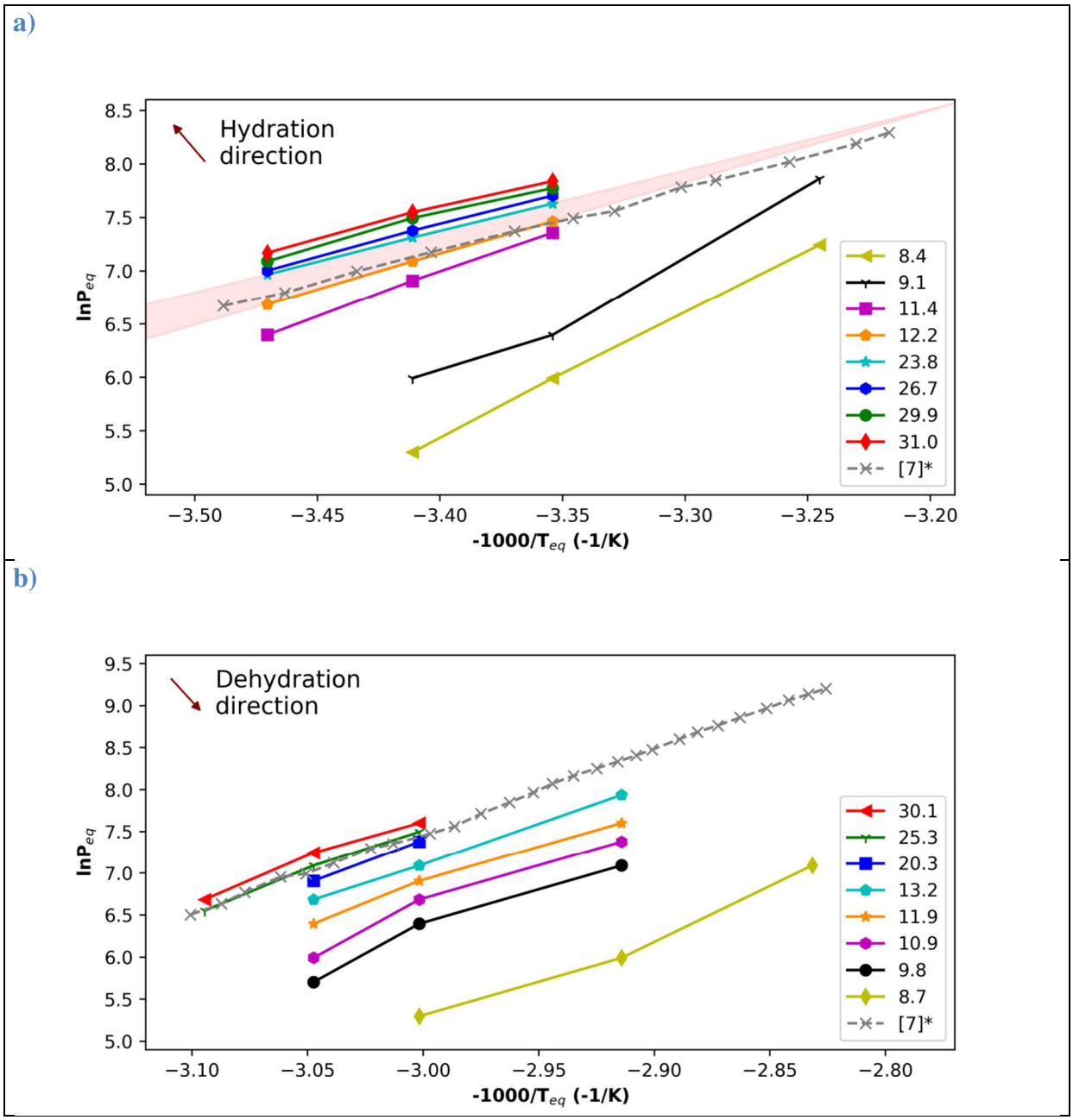

Figure 9. Thermodynamic equilibrium of ettringite hydration (a) and dehydration (b), in which [7]* is the reversible process of Met13 ↔ Ett30 adapted from [7].

4 Conclusions

The present work reports the thermal performance of ettringite for heat storage processes. The water vapor pressure and temperature are the two key parameters for the kinetics and thermodynamics of dehydration and hydration. Specially, the thermodynamics of hydration for meta-ettringite is separated into 3 stages: Met7.4 → Met12 → 24-hydrate → higher hydrates including EttX. While for dehydration, the 3 steps are: Ett30.6 →Ett30 → Met12 → Met6 in thermodynamics. The activation energy deduced for hydration reduced when the

409 water molecule number increasing. However, for dehydration, the values increase erratically
410 to 87.4 kJ/mol H_2O when n is as low as 8.7. In terms of the kinetics investigation, the removal
411 of water in ettringite is proved as stepwise at 80 °C in nitrogen, which is identical with its
412 crystal structure: Ett30.6 → Ett30 → Met18 → Met12 → Met7.5. Due to being a bi-variant
413 system for dehydration at high temperatures, this stepwise process is continuous without clear
414 plateaus for each stage. The temperature affects not only the rate of dehydration but also the
415 water removal degree: the higher the temperature is, the higher the rate and the water removal
416 degree are. For rehydration of ettringite, the over-absorption of water is very common when
417 the RH > 76 % without forming a liquid solution. The hydration enthalpy could be 1370
418 kJ/mol (~ 547 kWh/m^3) for forming Ett32.4 under the operating condition (20 °C and 90 %
419 RH), which is very competitive to other energy storage materials. Therefore, ettringite is very
420 suitable for storing thermal energy; especially during hydration, the no risk of forming an
421 apparent saturated solution makes it easy to control the variation of RH for hydration.

422 ## 5 Acknowledgements

423 The authors would like to appreciate the Association Nationale de la Recherche et de la
424 Technologie (ANRT) of France and LafargeHolcim Innovation Center for the funding of this
425 research. Dr. Bruno Huet from LafargeHolcim Innovation Center and Dr. Luis Guillermo
426 Baquerizo Ibarra are acknowledged for their meaningful discussions about thermal
427 characterization for the conversion between ettringite and meta-ettringite.

428 ## 6 References

429 [1] F. Kuznik; K. Johannes, Thermodynamic efficiency of water vapor / solid chemical
430 sorption heat storage for buildings: theoretical limits and integration considerations,
431 Appl. Sci. 10 (2020) 489. https://doi.org/10.20944/PREPRINTS201904.0079.V1.

432 [2] R. Clark, A. Mehrabadi, M. Farid, State of the art on salt hydrate thermochemical
433 energy storage systems for use in building applications, J. Energy Storage. 27 (2020)
434 101145.

435 [3] K.E. N'Tsoukpoe, T. Schmidt, H.U. Rammelberg, B.A. Watts, W.K.L. Ruck, A
436 systematic multi-step screening of numerous salt hydrates for low temperature
437 thermochemical energy storage, Appl. Energy. 124 (2014) 1–16.
438 https://doi.org/https://doi.org/10.1016/j.apenergy.2014.02.053.

439 [4] K. Ndiaye, M. Cyr, S. Ginestet, Durability and stability of an ettringite-based material
440 for thermal energy storage at low temperature, Cem. Concr. Res. 99 (2017) 106–115.
441 https://doi.org/https://doi.org/10.1016/j.cemconres.2017.05.001.

[5] J. Kaufmann, F. Winnefeld, Seasonal heat storage in calcium sulfoaluminate based hardened cement pastes – experiences with different prototypes, J. Energy Storage. 25 (2019).

[6] J. Kaufmann, F. Winnefeld, B. Lothenbach, Stability of ettringite in CSA cement at elevated temperatures, Adv. Cem. Res. 28 (2016) 251–261. https://doi.org/10.1680/jadcr.15.00029.

[7] L.G. Baquerizo, T. Matschei, K.L. Scrivener, Impact of water activity on the stability of ettringite, Cem. Concr. Res. 79 (2016) 31–44. https://doi.org/https://doi.org/10.1016/j.cemconres.2015.07.008.

[8] M. Cyr, S. Ginestet, K. Ndiaye, Energy storage/withdrawal system for a facility, 2015.

[9] B. Chen, F. Kuznik, M. Horgnies, K. Johannes, V. Morin, E. Gengembre, Physicochemical properties of ettringite/meta-ettringite for thermal energy storage: Review, Sol. Energy Mater. Sol. Cells. 193 (2019) 320–334. https://doi.org/https://doi.org/10.1016/j.solmat.2018.12.013.

[10] K. Ndiaye, S. Ginestet, M. Cyr, Experimental evaluation of two low temperature energy storage prototypes based on innovative cementitious material, Appl. Energy. 217 (2018) 47–55. https://doi.org/10.1016/J.APENERGY.2018.02.136.

[11] T. Grounds, H.G. Midgley, D. Nowell, The use of thermal methods to estimate the state of hydration of calciumtrisulphoaluminate hydrate $3CaO{\cdot}Al_2O_3{\cdot}3CaSO_4{\cdot}nH_2O$, Thermochim. Acta. 85 (1985) 215–218. https://doi.org/10.1016/0040-6031(85)85567-2.

[12] L.J. Struble, P.W. Brown, Heats of dehydration and specific heats of compounds found in concrete and their potential for thermal energy storage, Sol. Energy Mater. 14 (1986) 1–12. https://doi.org/https://doi.org/10.1016/0165-1633(86)90008-0.

[13] J.B. Ings, P.W. Brown, An evaluation of hydrated calcium aluminate compounds as energy storage media, NASA STI/Recon Tech. Rep. N. 83 (1982).

[14] N.N. Skoblinskaya, K.G. Krasilnikov, Changes in crystal structure of ettringite on dehydration. 1, Cem. Concr. Res. 5 (1975) 381–393. https://doi.org/https://doi.org/10.1016/0008-8846(75)90093-9.

[15] N.N. Skoblinskaya, K.G. Krasilnikov, L. V Nikitina, V.P. Varlamov, Changes in crystal structure of ettringite on dehydration. 2, Cem. Concr. Res. 5 (1975) 419–431. https://doi.org/https://doi.org/10.1016/0008-8846(75)90017-4.

[16] Y. Shimada, J.F. Young, Structural changes during thermal dehydration of ettringite, Adv. Cem. Res. 13 (2001) 77–81. https://doi.org/10.1680/adcr.2001.13.2.77.

[17] S. Mantellato, M. Palacios, R.J. Flatt, Impact of sample preparation on the specific surface area of synthetic ettringite, Cem. Concr. Res. 86 (2016) 20–28. https://doi.org/https://doi.org/10.1016/j.cemconres.2016.04.005.

[18] B. Chen, M. Horgnies, B. Huet, V. Morin, K. Johannes, F. Kuznik, Comparative kinetics study on carbonation of ettringite and meta-ettringite based materials, Cem. Concr. Res. 137 (2020) 106209. https://doi.org/https://doi.org/10.1016/j.cemconres.2020.106209.

[19] K. Kira, Y. Makino, Y. Murata, Dehydration and Rehydration of Ettringite, Gypsum Lime. 1981 (1981) 7–13. https://doi.org/10.11451/mukimate1953.1981.7.

[20] Q. Zhou, F.P. Glasser, Thermal stability and decomposition mechanisms of ettringite at <120°C, Cem. Concr. Res. 31 (2001) 1333–1339. https://doi.org/https://doi.org/10.1016/S0008-8846(01)00558-0.

[21] L.J. Struble, P.W. Brown, Evaluation of ettringite and related compounds for use in solar energy storage, Prog. Rep. Natl. Bur. Stand. Washington, DC. Cent. Build. Technol. (1984).

[22] H. Pollmann, Characterization of different water contents of ettringite and kuzelite, in: Proc. 12th Int. Congr. Chem. Cem. Montr. Canada, 2007.

[23] J.G.D. Preturlan, L. Vieille, S. Quiligotti, L. Favergeon, Comprehensive Thermodynamic Study of the Calcium Sulfate-Water Vapor System. Part 1: Experimental Measurements and Phase Equilibria, Ind. Eng. Chem. Res. 58 (2019) 9596–9606. https://doi.org/10.1021/acs.iecr.9b00856.